Carrier density control of magnetism and Berry phases in doped $EuTiO_3$

Kaveh Ahadi, Zhigang Gui, Zach Porter, Jeffrey W. Lynn, Zhijun Xu, Stephen D. Wilson, Anderson Janotti, and Susanne Stemmer

Citation: APL Materials **6**, 056105 (2018); doi: 10.1063/1.5025317
View online: https://doi.org/10.1063/1.5025317
View Table of Contents: http://aip.scitation.org/toc/apm/6/5
Published by the American Institute of Physics

Carrier density control of magnetism and Berry phases in doped $EuTiO_3$

Kaveh Ahadi,[1,a] Zhigang Gui,[2] Zach Porter,[1] Jeffrey W. Lynn,[3] Zhijun Xu,[3,4] Stephen D. Wilson,[1] Anderson Janotti,[2] and Susanne Stemmer[1]
[1]*Materials Department, University of California, Santa Barbara, California 93106-5050, USA*
[2]*Department of Materials Science and Engineering, University of Delaware, Newark, Delaware 19716-3106, USA*
[3]*NIST Center for Neutron Research, National Institute of Standards and Technology, Gaithersburg, Maryland 20899, USA*
[4]*Department of Materials Science and Engineering, University of Maryland, College Park, Maryland 20742, USA*

(Received 8 February 2018; accepted 30 April 2018; published online 17 May 2018)

In materials with broken time-reversal symmetry, the Berry curvature acts as a reciprocal space magnetic field on the conduction electrons and is a significant contribution to the magnetotransport properties, including the intrinsic anomalous Hall effect. Here, we report neutron diffraction, transport, and magnetization measurements of thin films of doped $EuTiO_3$, an itinerant magnetic material, as a function of carrier density and magnetic field. These films are itinerant antiferromagnets at all doping concentrations. At low carrier densities, the magnetoresistance indicates a metamagnetic transition, which is absent at high carrier densities ($>6 \times 10^{20}$ cm^{-3}). Strikingly, the crossover coincides with a sign change in the spontaneous Hall effects, indicating a sign change in the Berry curvature. We discuss the results in the context of the band structure topology and its coupling to the magnetic texture.
https://doi.org/10.1063/1.5025317

A major triumph of 21st century condensed matter theory is the description of the anomalous Hall effect (AHE)[1] of itinerant magnetic materials in terms of the Berry phase of the quasiparticles on the Fermi surface.[2–6] For example, sign changes in the Hall effect of itinerant ferromagnets can be explained with the proximity of the Fermi level to magnetic monopoles in momentum space (band crossings or Weyl points), which act as sources/drains of the Berry curvature.[7,8] The Berry phase interpretation also elegantly explains recently discovered, strong AHEs in antiferromagnets.[9–11] In addition, chiral spin structures can cause a second, distinct contribution to the Hall resistance, the topological Hall effect (THE), which is due to the real space magnetic texture.[12–17] Unlike the AHE, the THE does not require spin-orbit coupling.[18] The topological picture of these Hall effects presents a powerful experimental tool to study interactions between electronic and spin structures, a question that is central to many unusual phenomena in quantum materials.

A particularly interesting system for such studies is doped $EuTiO_3$, an itinerant magnet whose carrier density and thus the Fermi level can be tuned over a wide range by chemical doping with trivalent rare earth ions. Stoichiometric $EuTiO_3$ is a G-type antiferromagnet with spins ordering on the Eu sites [$4f^7$ (S = 7/2)] at the Néel temperature (T_N) of 5.5 K.[19,20] Doping with rare earth ions produces an itinerant magnet with conduction electrons residing in the Ti d-states.[21] Its AHE exhibits a sign change at a critical carrier density.[22] Recently, the THE was observed in Sm-doped $EuTiO_3$ films,[23] suggesting a chiral spin texture.

Here, we show that the sign of both Hall effects is controlled by doping and intimately coupled to the appearance of other field-induced phenomena, in particular, metamagnetic transitions.

[a]Author to whom correspondence should be addressed: kahadi@mrl.ucsb.edu

In combination with band structure calculations using density functional theory (DFT), the results suggest a strong connection between the band topology and these phenomena.

Approximately 50-nm-thick (unless stated otherwise), epitaxial $EuTiO_3$ layers were grown by molecular beam epitaxy on (001) $(La_{0.3}Sr_{0.7})(Al_{0.65}Ta_{0.35})O_3$ (LSAT) single crystals.[23] Films were doped with different amounts of Sm to obtain Hall carrier densities at room temperature (n_{RT}) of 1.2×10^{20} cm^{-3}, 3.4×10^{20} cm^{-3}, 6.5×10^{20} cm^{-3}, and 8.7×10^{20} cm^{-3}, respectively, unless stated otherwise. The Hall mobilities of these films at 2 K were 97 cm^2/V s, 167 cm^2/V s, 34 cm^2/V s, and 20 cm^2/V s, respectively. Thicker (100 nm) films showed 2 K mobilities up to 220 cm^2/V s. Electron beam evaporation through a shadow mask was used to deposit Au/Ti (400/40 nm) contacts for Hall and resistance measurements using square Van der Pauw structures. Magnetotransport measurements as a function of temperature were carried out using a Quantum Design Physical Property Measurement System (PPMS). Magnetic properties were measured using a Quantum Design superconducting quantum interface device (SQUID) magnetometer. While the stoichiometric $EuTiO_3$ film is highly resistive, the Sm-doped films are metallic down to liquid helium temperature (see the supplementary material).

Neutron diffraction measurements on thicker (100 nm) $EuTiO_3$ films were performed using the triple-axis spectrometer (BT-7 at the NIST Center for Neutron Research[24]). Measurements were taken with the initial and final neutron energies of 14.7 meV (wavelength 2.359 Å) fixed with a pyrolitic graphite (PG) monochromator and analyzer. One PG filter was placed before the sample and two after the sample, and the collimator configuration was open-50′-50′-120′ before the monochromator, sample, analyzer, and single detector, respectively. Samples were oriented in the [h 0 l] scattering plane and mounted within a closed cycle refrigerator. A tetragonal unit cell is used to reference the $EuTiO_3$ unit cell in the neutron measurements. Uncertainties indicated represent one standard deviation in the data.

Density functional theory (DFT) calculations were carried out using the VASP code (VASP)[25] within the projected augmented wave method.[26] The general gradient approximation (GGA) using the PBEsol parameterization[27] was adopted for the exchange-correlation potential with an on-site Coulomb interaction added to the localized Eu 4f bands in the DFT + U approach.[28] The values of on-site Coulomb interaction parameters were set to U = 8.0 eV and J = 1.0 eV. This approach corrects the position of the Eu 4f band with respect to the Ti 3d band. For all calculations, we used a plane-wave basis set with an energy cutoff of 550.0 eV. Integrations over the Brillouin zone were performed using $7 \times 7 \times 5$ Monkhorst-Pack k-point mesh, and the structures were fully relaxed until the forces on each atom were less than 0.005 eV/A and total energy differences between consecutive steps were less than 10^{-7} eV.

All samples, independent of their carrier density, showed an upturn in the longitudinal resistance (R_{xx}) at ~20 K, with a peak at ~6 K, signifying the transition to long-range magnetic order (see the supplementary material). Notably, the transition temperature is close to T_N of stoichiometric $EuTiO_3$ and decreases only slightly with carrier density. This is also confirmed by the neutron diffraction data, shown in Fig. 1. Magnetic Bragg peaks at tetragonal [odd, 0, odd] (pseudocubic [1/2 1/2 1/2]-type) indices were observed in all samples below T_N. These magnetic peaks are indicative of persistent antiferromagnetic order with carrier substitution.

Figure 2 shows the longitudinal resistance, R_{xx}, as a function of the out-of-plane magnetic field (B) at 2 K, 5 K, 10 K, and 15 K, respectively. Here, B was swept from +6 T to −6 T and back. The film with the highest carrier density ($n_{RT} = 8.7 \times 10^{20}$ cm^{-3}) shows negative magnetoresistance below the transition temperature and hysteresis, consistent with previous studies.[21–23] The hysteresis is reduced for the sample with $n_{RT} = 6.5 \times 10^{20}$ cm^{-3} and disappears completely for the samples with lower carrier densities, $n_{RT} = 3.4 \times 10^{20}$ cm^{-3} and $n_{RT} = 1.2 \times 10^{20}$ cm^{-3}, respectively. Furthermore, the low-temperature magnetoresistance behavior of the low doped samples is also completely different. These samples exhibit pronounced positive magnetoresistance at low B (<3 T), followed by an abrupt change to negative magnetoresistance at higher B. This indicates an abrupt, magnetic-field-induced transition to a new magnetic state in these samples. The positive magnetoresistance, although weaker, is still present even with B in-plane (see the supplementary material). Although the magnetoresistance does not show hysteresis, a small magnetization can be detected upon field cooling the film with $n_{RT} = 3.4 \times 10^{20}$ cm^{-3}, as shown in Fig. 3(a), which also shows a small hysteresis at 2 K [Fig. 3(b)].

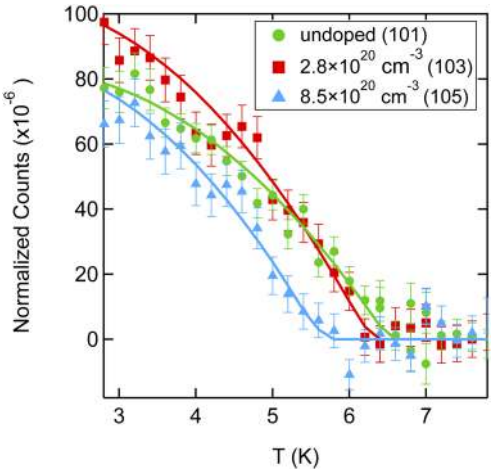

FIG. 1. Neutron diffraction intensities of the magnetic [1 0 L] reflections as a function of temperature for samples with varying carrier concentrations. Intensities are normalized by the [103] substrate reflection intensity and have the incoherent background removed. Solid lines represent simple mean-field order parameters fits to the data.

The magnetization increases, and the hysteresis is slightly more pronounced in the higher doped samples [Figs. 3(a) and 3(c)].

Figure 4 shows the AHE and THE contributions to the Hall resistance (R_{xy}) for the films with different carrier concentrations at T = 2 K. The raw data were antisymmetrized to eliminate the longitudinal magnetoresistance contribution, i.e., $R_{xy} = \left[R_{xy}{}^{raw}(+B) - R_{xy}{}^{raw}(-B)\right]/2$. In the presence of an AHE and/or a THE, R_{xy} is given by $R_{xy} = R_0H + R_{AHE} + R_{THE}$, where R_{AHE} and R_{THE} are the AHE and THE contributions, respectively.[12] Linear fits at high B (6 T–9 T) yield the

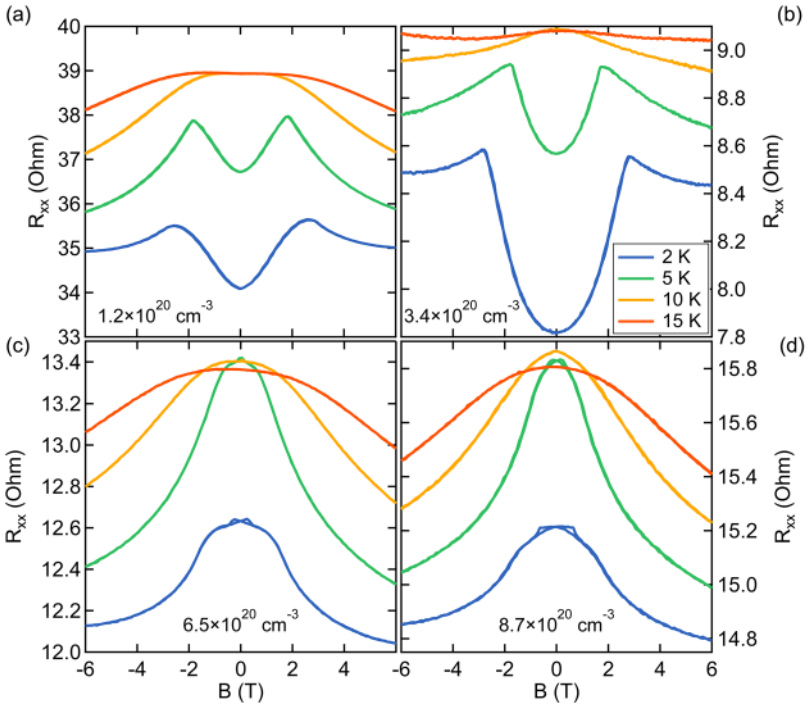

FIG. 2. Magnetoresistance of doped $EuTiO_3$ films having room temperature carrier densities of 1.2 × 10^{20} cm^{-3}, 3.4 × 10^{20} cm^{-3}, 6.5 × 10^{20} cm^{-3}, and 8.7 × 10^{20} cm^{-3}, respectively, measured at (a) 2 K, (b) 5 K, (c) 10 K, and (d) 15 K.

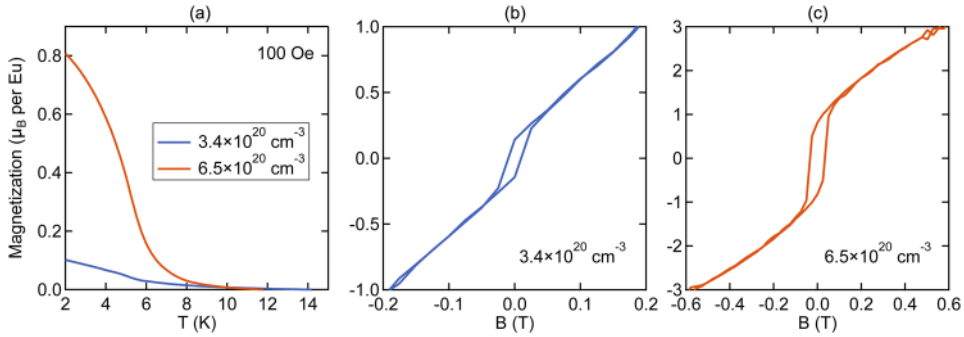

FIG. 3. Magnetization measurements of $EuTiO_3$ films having room temperature carrier densities of 3.4×10^{20} cm^{-3} and 6.5×10^{20} cm^{-3}, respectively. (a) Magnetization as a function of temperature under field cooling (10 mT). [(b) and (c)] Magnetization at 2 K as a function of B for the samples with carrier densities of (b) 3.4×10^{20} cm^{-3} and (c) 6.5×10^{20} cm^{-3}. Here, B was normal to the film plane.

ordinary Hall component (R_0B), which was subtracted from the data shown in Fig. 4. The monotonic contribution that extrapolates to zero at a low temperature is the AHE. A non-monotonic contribution is apparent as peaks or valleys and resembles a THE.[3] The lowest doped sample with $n_{RT} = 1.2 \times 10^{20}$ cm^{-3} shows only a small non-monotonic contribution [Fig. 4(a)]. At a higher carrier density, $n_{RT} = 3.4 \times 10^{20}$ cm^{-3}, this component becomes dominant compared to the monotonic AHE signal [Fig. 4(b)]. It vanishes near the field for the metamagnetic transition, as expected for a transition to ferromagnetic, collinear alignment. Increasing the carrier concentration ($n_{RT} = 6.5 \times 10^{20}$ cm^{-3} and 8.7×10^{20} cm^{-3}) causes a sign change in both contributions [Figs. 4(c) and 4(d)]. Furthermore, two peaks can be detected for these samples. The peak at ~0.8 T (stronger in upward than in

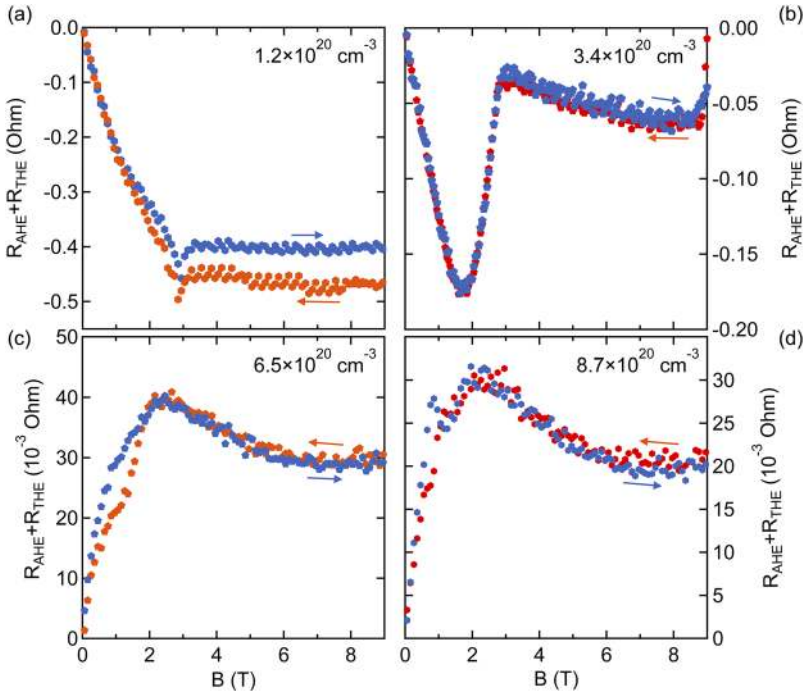

FIG. 4. Hall resistances of doped $EuTiO_3$ films having room temperature carrier densities of 1.2×10^{20} cm^{-3}, 3.4×10^{20} cm^{-3}, 6.5×10^{20} cm^{-3}, and 8.7×10^{20} cm, respectively. The measurements were carried out at 2 K as a function of field, and the data shown are after anti-symmetrization and subtraction of the ordinary (linear in B) Hall component. For temperature dependent data of the highest doped sample, see Ref. 23.

downward sweep) is near the field at which the closure of the hysteresis is seen in the magnetoresistance data (Fig. 2). The second, more pronounced peak at ~2 T has no corresponding feature in the magnetoresistance.

We next discuss the results. As a function of carrier density, the films transition from a low magnetization state to a higher magnetization state, displaying signatures, such as a small hysteresis, of a canted antiferromagnet. Beyond that, however, there are relatively little changes in terms of the magnetic state in the absence of a magnetic field. Doped $EuTiO_3$ thus joins a growing list of antiferromagnets that exhibit spontaneous Hall effects even though they have only a small net magnetization,[15,29] consistent with the Berry phase origin and indicative of a non-collinear spin arrangement.[9–11,30]

In contrast to the nearly doping insensitive T_N, dramatic differences exist in the magnetotransport behavior under applied magnetic fields and, here, the response critically depends on the carrier density (position of the Fermi level). They include sign changes in the spontaneous Hall effects and the (dis)appearance of the metamagnetic transition (sign change in the magnetoresistance). These responses do *not* gradually evolve with carrier density but rather exhibit a *cross-over* behavior at a carrier density of 4-5 $\times$ 10^{20} cm^{-3}. We note that these changes in the Hall effect are due to the intrinsic, Berry phase contribution. While the longitudinal conductivity changes drastically as a function of carrier concentration (~10^4-10^5 Ω^{-1} cm^{-1}), the magnitude of the Hall conductivity remains fairly constant (~10^3 Ω^{-1} cm^{-1}) (see the supplementary material). A weak dependence of the Hall conductivity on the longitudinal conductivity is a hallmark of intrinsic dissipationless topological Berry curvature contribution.[31]

A sign change in the intrinsic AHE with doping is known to be a signature of the Fermi level crossing a Weyl node.[7] Indeed, DFT calculations of band structures of electron-doped, ferromagnetic $EuTiO_3$ (Fig. 5) show band crossings that indicate the presence of Weyl points in the conduction band. For instance, a Ti-3*d* conduction band with spin-up crosses another Ti-3*d* conduction-band with spin-down at ~24% along the Γ-X (in-plane) direction, in a spin-momentum locked configuration. Changing the electron density from 3.4 $\times$ 10^{20} to 6.2 $\times$ 10^{20} cm^{-3}, where we observe the crossover in the magnetic characteristics and the sign changes in the Hall effects, is predicted in these calculations to result in the Fermi level located near this crossing point. Such crossings give large contributions to the Berry curvature in *k*-space and to the intrinsic anomalous Hall conductivity,[3,7,32] explaining the experimental observations.

The present results thus link the presence of a Weyl point to the presence of a field-induced magnetic transition. High carrier density films (Fermi level above the Weyl point) display only negative magnetoresistance. The latter is typical of scattering of itinerant electrons from localized spins, which reduces as the spins align in the magnetic field.[21] This indicates that in these films, the magnetic field only gradually drives a non-collinear spin structure toward a more collinear one.

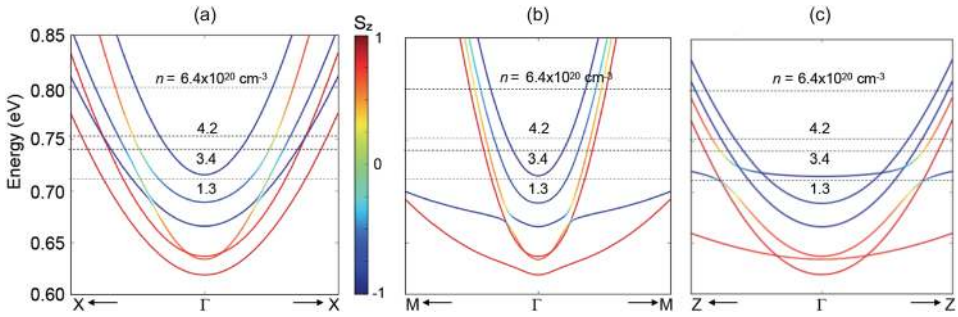

FIG. 5. Band structures for doped $EuTiO_3$ along (a) Γ-X, (b) Γ-M, and (c) Γ-Z high symmetry lines in the Brillouin zone of the 20-atom tetragonal cell. The projections on the spin *z*-component (Sz) are indicated by the color of the lines: red corresponds to Sz = +1 and blue to Sz = −1. For these bands, the Sx and Sy projections are negligible. The dashed lines indicate the Fermi level position for four electron concentrations (1.2, 3.4, 4.2, and 6.4 $\times$ 10^{20} cm^{-3}) at zero temperature. The energy of the bottom of conduction band is set to zero. The boundaries in the wave vectors correspond to ±1/3 (π/a, 0, 0) along Γ-X, ±1/3 (π/*a*, π/*a*, 0) along Γ-M, and ±1/3 (0, 0, π/*c*) along Γ-Z, where *a* and *c* are the lattice parameters of the 20-atom tetragonal unit cell.

Films with low carrier densities, however, exhibit a metamagnetic transition. The interpretation of a metamagnetic transition is supported by a sharp transition from positive to negative magnetoresistance at the same field that causes the non-monotonic contribution to the Hall effect to vanish. We note that the positive magnetoresistance is strongly associated with the magnetic order at low carrier densities since it only appears below T_N. While metamagnetic transitions are often associated with the Fermi level being located near a singularity in the density of states and a Lifshitz transition of the Fermi surface,[33,34] the presence of a Weyl point in an antiferromagnetic material presents an alternative mechanism. In particular, as the magnetic field reorients the spins, it can modify the band topology[35] and thereby affect the Hall and magnetotransport. In general, Lifshitz transitions can give rise to magnetic-field-tuned quantum criticality[36,37] and signatures of this might appear in transport. Here, we have analyzed the A-parameter, which characterizes the amplitude of the temperature dependent part of the electrical resistance and which is proportional to the effective mass.[38] This A-parameter is enhanced near the magnetic field-induced transition of the sample with $n_{RT} = 3.4 \times 10^{20}$ cm^{-3} (see the supplementary material). Mass enhancement is a signature of a quantum critical point.[38]

Finally, we comment on the sign change in the non-monotonous spontaneous Hall effect. A THE is a signature of the real space Berry phase due to a non-coplanar spin texture,[17] but, in practice, the THE and AHE might be difficult to distinguish.[35] It is clear, however, that this signal vanishes as the magnetic field aligns the spins into a collinear configuration and that it is still present even in the samples were the magnetoresistance does not show the abrupt transition with the magnetic field. These findings support the interpretation in terms of a THE. A sign change then indicates a change in the spin chirality,[39] suggesting an interesting connection to the specifics of the band topology.

In summary, doped, itinerant $EuTiO_3$ is proving to be a highly tunable system to investigate the relationship between Weyl points, spontaneous Hall effects, and novel, magnetic field driven transitions. Theoretical studies of these transitions, and how they are associated with changes in the spin alignments and how they contribute to the magnetotransport, will be required for a complete understanding of the results reported here and should be an interesting contribution to the emerging field of topological antiferromagnetic spintronics.[35]

See supplementary material for an analysis of the Hall and longitudinal conductivities with doping, sheet resistances as a function of temperature and magnetic field and magnetic field orientation, Hall carrier densities data as a function of temperature, and an analysis of the temperature coefficient (A-parameter) of the electrical resistance.

We acknowledge support from the U.S. Army Research Office (No. W911NF-14-1-0379) and the U.S. National Science Foundation under DMREF Award No. 1729489. The work made use of the MRL Shared Experimental Facilities, which are supported by the MRSEC Program of the U.S. National Science Foundation under Award No. DMR 1720256. S.D.W and Z.P. thank Ryan Need for helpful assistance in neutron scattering measurements. Z.G. and A.J. were supported by the National Science Foundation under Grant No. 1652994. The calculations were performed using the Extreme Science and Engineering Discovery Environment (XSEDE) supercomputer facility, which is supported by National Science Foundation Grant No. ACI-1053575 under the allocation No. TG-DMR-150099. Identification of any commercial product or trade name does not imply endorsement or recommendation by the National Institute of Standards and Technology.

[1] R. Karplus and J. M. Luttinger, Phys. Rev. **95**, 1154 (1954).
[2] T. Jungwirth, Q. Niu, and A. H. MacDonald, Phys. Rev. Lett. **88**, 207208 (2002).
[3] M. Onoda and N. Nagaosa, J. Phys. Soc. Jpn. **71**, 19 (2002).
[4] F. D. M. Haldane, Phys. Rev. Lett. **93**, 206602 (2004).
[5] N. Nagaosa, J. Sinova, S. Onoda, A. H. MacDonald, and N. P. Ong, Rev. Mod. Phys. **82**, 1539 (2010).
[6] J. W. Ye, Y. B. Kim, A. J. Millis, B. I. Shraiman, P. Majumdar, and Z. Tesanovic, Phys. Rev. Lett. **83**, 3737 (1999).
[7] Z. Fang, N. Nagaosa, K. S. Takahashi, A. Asamitsu, R. Mathieu, T. Ogasawara, H. Yamada, M. Kawasaki, Y. Tokura, and K. Terakura, Science **302**, 92 (2003).
[8] R. Mathieu, A. Asamitsu, H. Yamada, K. S. Takahashi, M. Kawasaki, Z. Fang, N. Nagaosa, and Y. Tokura, Phys. Rev. Lett. **93**, 016602 (2004).
[9] H. Chen, Q. Niu, and A. H. MacDonald, Phys. Rev. Lett. **112**, 017205 (2014).
[10] J. Kubler and C. Felser, Europhys. Lett. **108**, 67001 (2014).
[11] R. Shindou and N. Nagaosa, Phys. Rev. Lett. **87**, 116801 (2001).

[12] N. Nagaosa and Y. Tokura, Nat. Nanotechnol. **8**, 899 (2013).
[13] A. Neubauer, C. Pfleiderer, B. Binz, A. Rosch, R. Ritz, P. G. Niklowitz, and P. Boni, Phys. Rev. Lett. **102**, 186602 (2009).
[14] K. Ohgushi, S. Murakami, and N. Nagaosa, Phys. Rev. B **62**, R6065 (2000).
[15] C. Surgers, G. Fischer, P. Winkel, and H. V. Lohneysen, Nat. Commun. **5**, 3400 (2014).
[16] Y. Taguchi, Y. Oohara, H. Yoshizawa, N. Nagaosa, and Y. Tokura, Science **291**, 2573 (2001).
[17] C. Franz, F. Freimuth, A. Bauer, R. Ritz, C. Schnarr, C. Duvinage, T. Adams, S. Blugel, A. Rosch, Y. Mokrousov, and C. Pfleiderer, Phys. Rev. Lett. **112**, 186601 (2014).
[18] P. Bruno, V. K. Dugaev, and M. Taillefumier, Phys. Rev. Lett. **93**, 096806 (2004).
[19] T. R. McGuire, M. W. Shafer, R. J. Joenk, H. A. Alperin, and S. J. Pickart, J. Appl. Phys. **37**, 981 (1966).
[20] V. Scagnoli, M. Allieta, H. Walker, M. Scavini, T. Katsufuji, L. Sagarna, O. Zaharko, and C. Mazzoli, Phys. Rev. B **86**, 094432 (2012).
[21] T. Katsufuji and Y. Tokura, Phys. Rev. B **60**, R15021 (1999).
[22] K. S. Takahashi, M. Onoda, M. Kawasaki, N. Nagaosa, and Y. Tokura, Phys. Rev. Lett. **103**, 057204 (2009).
[23] K. Ahadi, L. Galletti, and S. Stemmer, Appl. Phys. Lett. **111**, 172403 (2017).
[24] J. W. Lynn, Y. Chen, S. Chang, Y. Zhao, S. Chi, W. Ratcliff, B. G. Ueland, and R. W. Erwin, J. Res. Natl. Inst. Stand. Technol. **117**, 61 (2012).
[25] G. Kresse and J. Furthmuller, Phys. Rev. B **54**, 11169 (1996).
[26] P. E. Blochl, Phys. Rev. B **50**, 17953 (1994).
[27] J. P. Perdew, A. Ruzsinszky, G. I. Csonka, O. A. Vydrov, G. E. Scuseria, L. A. Constantin, X. L. Zhou, and K. Burke, Phys. Rev. Lett. **100**, 136406 (2008).
[28] V. I. Anisimov, F. Aryasetiawan, and A. I. Lichtenstein, J. Phys.: Condens. Matter **9**, 767 (1997).
[29] S. Nakatsuji, N. Kiyohara, and T. Higo, Nature **527**, 212 (2015).
[30] B. Göbel, A. Mook, J. Henk, and I. Mertig, Phys. Rev. B **95**, 094413 (2017).
[31] S. Onoda, N. Sugimoto, and N. Nagaosa, Phys. Rev. B **77**, 165103 (2008).
[32] X. J. Wang, J. R. Yates, I. Souza, and D. Vanderbilt, Phys. Rev. B **74**, 195118 (2006).
[33] D. J. Singh and I. I. Mazin, Phys Rev. B **63**, 165101 (2001).
[34] B. Binz and M. Sigrist, Europhys. Lett. **65**, 816 (2004).
[35] L. Šmejkal, Y. Mokrousov, B. Yan, and A. H. MacDonald, Nat. Phys. **14**, 242 (2018).
[36] S. A. Grigera, R. S. Perry, A. J. Schofield, M. Chiao, S. R. Julian, G. G. Lonzarich, S. I. Ikeda, Y. Maeno, A. J. Millis, and A. P. Mackenzie, Science **294**, 329 (2001).
[37] R. S. Perry, L. M. Galvin, S. A. Grigera, L. Capogna, A. J. Schofield, A. P. Mackenzie, M. Chiao, S. R. Julian, S. I. Ikeda, S. Nakatsuji, Y. Maeno, and C. Pfleiderer, Phys. Rev. Lett. **86**, 2661 (2001).
[38] A. J. Schofield, Contemp. Phys. **40**, 95 (1999).
[39] Y. Taguchi, T. Sasaki, S. Awaji, Y. Iwasa, T. Tayama, T. Sakakibara, S. Iguchi, T. Ito, and Y. Tokura, Phys. Rev. Lett. **90**, 257202 (2003).